Corrosion behavior of P92 in supercritical water

Kaiju Yin[a], Shaoyu Qiu[a], Rui Tang[a,] *, Qiang Zhang[a], Lefu Zhang[b]

[a] National Key Lab. For Nuclear Fuel and Materials, Nuclear Power Institute of China, P.O. Box 436, Chendu 610042, PR China

[b]School of Nuclear Science and Engineering, Shanghai Jiao Tong University, Shanghai 200240, PR China

*Corresponding author. Tel: +86 28 8590 3862, Fax: +86 28 8590 6023.

E-mail address: xajttr@163.com (Rui Tang)

Abstract

The corrosion behavior of a ferritic/martensitic steel P92 exposed to supercritical water (SCW) at 500 to 600 ℃ and 25 MPa was investigated by means of gravimetry, scanning electron microscope/energy dispersive X-ray spectroscopy and X-ray diffraction. A dual-layered oxide scale, which was mainly composed of an outer magnetite layer and an inner magnetite/spinel-mixed layer, formed on P92. The initial oxide scale was rather porous, while the porosity decreased with an increase of exposure time. Oxidation rates at three different temperatures followed a parabolic law. The oxidation at 600 ℃ was so severe that cracks occurred along grain boundaries in the oxide scale. A probable corrosion mechanism for P92 exposed to SCW was proposed based on the above observations, focusing on oxide formation by oxygen absorption without any metallic dissolution.

Keywords: Ferritic/martensitic steel; Supercritical water; Oxidation; Oxide scale

1. Introduction

The supercritical water reactor (SCWR) design has been selected as one of the reactor concepts for future Generation IV nuclear reactor systems, because of its simplified design, smaller volume and higher thermal efficiency than current light water reactors (LWRs) [1-3]. However, above the thermodynamic critical point (374.2 ? and 22.1 MPa), the supercritical water (SCW) coolant is expected to be more corrosive to structural materials that are commonly used in nuclear reactors and fossil power plants[4, 5]. In order to put the SCWR design into practice, experimental evaluation of proposed structural materials is urgently needed. Ferritic/martensitic (F/M) steels, austenitic stainless steels and Ni-based alloys are considered as candidates for future SCWR systems [6-17]. Among these classes of alloys, austenitic steels generally have a relatively low thermal conductivity, high thermal expansion coefficient, and poor weldability. The Ni-based alloys also have low thermal conductivity. More importantly, these two categories of alloys contain substantial amounts of Ni, which is susceptible to transmutation under the influence of irradiation [6]. Consequently, low Ni or Ni-free F/M steels present an attractive alternative. Elevated-temperature F/M steels are expected for in-core (cladding and ducts) and out-of-core (pressure vessel, piping, etc.) applications [1], since F/M steels with body centered cubic structure provide good swelling resistance, low thermal expansion coefficient and high thermal conductivity.

The 9-12% Cr F/M steels, such as P91 and P92, exhibit good processing ability and mechanical properties, combined with satisfactory corrosion resistance at elevated

temperatures [15]. Compared with P91, P92 shows improved high-temperature mechanical properties, especially a 10~20% increase in creep strength at 600 ℃ for 100, 000 h [19, 20], which is attributed to solution strengthening by W and Mo additions, and precipitation strengthening by V and Nb additions. Unlike P91, only a few investigations of the corrosion of P92 in SCW have been carried out. Based on cross-sectional TEM observations, Jang found that two 9Cr steels followed parabolic oxidation kinetics in SCW, and the scale consisted of three distinctive layers, namely Fe_3O_4, $(Fe, Cr)_3O_4$, and an internally oxidized zone [21]. Through glow discharge optical emission spectroscopy analyses, Bojinov identified a dual-layered oxide film on P92H steel exposed to SCW, with a high Cr concentration in the inner layer [22]. More investigations of the corrosion of P92 in SCW are necessary for SCWR development.

The present work investigates the corrosion performance of P92 exposed to SCW at 500 to 600 ℃ under a pressure of 25 MPa, to at evaluate the corrosion behavior of P92 as a promising candidate material for the SCWR.

2. Experimental

The F/M steel P92 test material was supplied by Panzhihua Iron & Steel Corporation, and had been annealed at 1050 ℃ for 30 min and tempered at 780 ℃ for 60 min. The nominal chemical composition tested by X-ray fluorescence spectroscopy (XRF) is listed in Table 1. The as-received P92 stock was first cut into test samples with a dimension of about 40 mm × 20 mm × 1.5 mm and then mechanically polished to a 1 μm diamond finish. Then the samples were cleaned with

acetone and ultrasonically rinsed with de-ionized water for 5 min.

Table 1 Chemical composition (wt.%) of the tested material by XRF

C	Si	Mn	Cr	Al	Nb	B	Ni	Cu	Mo	W	V	P	S	N	Fe
0.13	*0.50*	*0.50*	*9.50*	*0.04*	*0.09*	*0.001*	*0.40*	*0.25*	*0.60*	*2.0*	*0.25*	*0.02*	*0.01*	*0.03*	*bal.*

All SCW exposure tests were performed in a 2 L autoclave at 500, 550 and 600 ℃ respectively, at a pressure of 25 MPa for time periods up to 1000 h. For the inlet water, the dissolved oxygen concentration was controlled below 10 ppb by bubbling pure nitrogen through it, while the water conductivity (at 25 ℃) was kept under 0.1 μS/cm.

After completion of each exposure period, the corrosion resistance was evaluated by gravimetry, as well as surface and cross-sectional analyses. An ESJ180-4 electric balance, with an accuracy of 0.1 mg, was used to make weight change measurements. An FEI Nano 400 scanning electron microscope (SEM), equipped with energy dispersive X-ray spectroscopy (EDS), was employed to observe oxide morphology and analyze its chemical composition across the oxide thickness. Surface oxide phases were identified by a Philips X' Pert PRO MRD X-ray diffractometer (XRD) with a Cu kα radiation source.

3. Results and discussion

The plan-view images of SCW-exposed samples are shown in Fig. 1. The initial oxide scale had a rather high porosity, which decreased along with the exposure time. It is proposed that the formation of the pores is related to the defect types present in

the magnetite structure [23, 24]. There are two major defect types in magnetite, namely interstitial Fe^{2+}

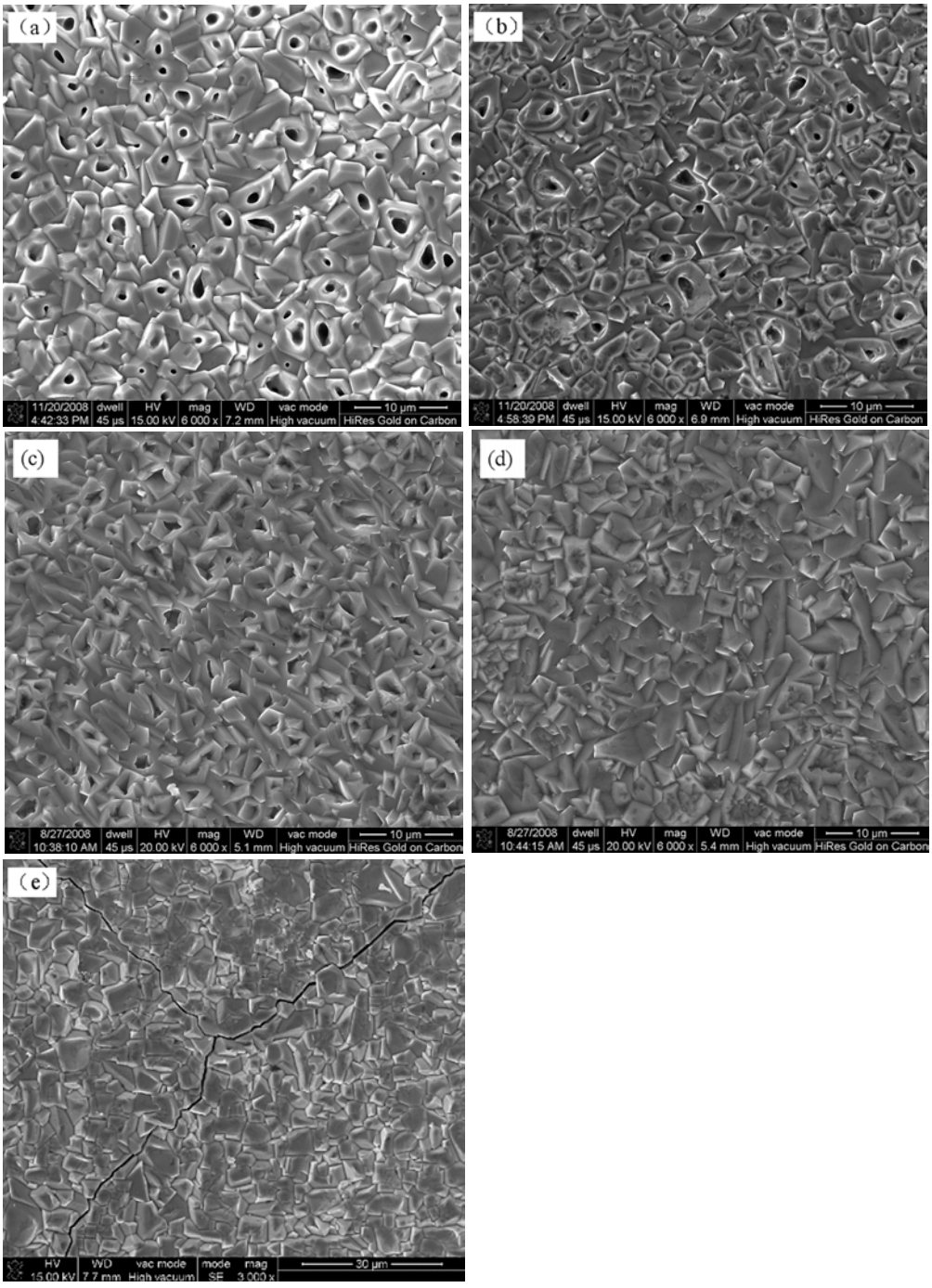

Fig. 1 SEM images of the surface morphology of the samples exposed to SCW under a pressure of 25 MPa (a) at 500 ℃ for 200 h, (b) at 500 ℃ for 800 h, (c) at 550 ℃ for 200 h, (d) at 550 ℃ for 800 h, (e) at 600 ℃ for 200 h.

and vacancies, which may collapse into pores if the concentration is high enough. In

Fe-Cr alloys, oxides grow predominantly by outward diffusion of cations and inward diffusion of oxygen, which is probably affected by short circuit paths such as pores,

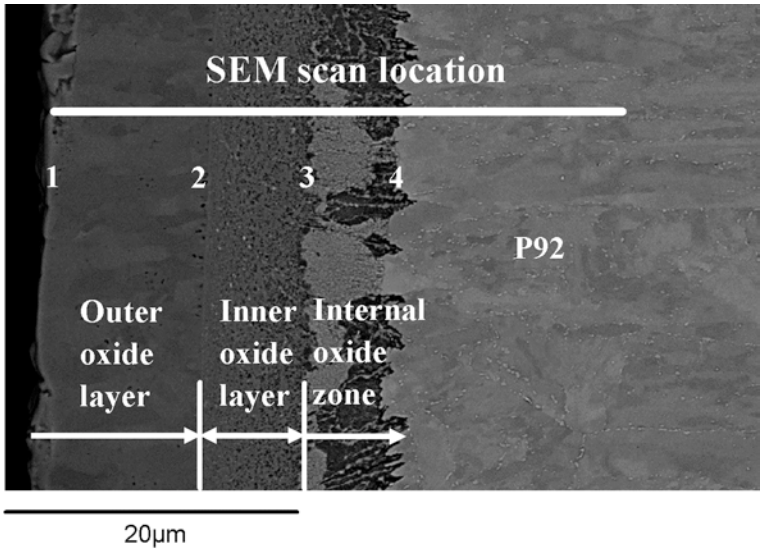

Fig. 2 Cross-sectional SEM image of the sample exposed to SCW at 550 ℃ and 25 MPa for 1000 h.

cracks and grain boundaries [25, 26]. The decrease in the number of pores indicates their weakening influence on the diffusion of cations and oxygen. All the samples formed uniform and adhesive scales without any evidence of exfoliation, while the test temperature played an important role in the integrity of the oxide scales. At 500 and 550 ℃, no cracks occurred in the scales. However, at 600 ℃, cracks occurred along oxide grain boundaries in the scale, as illustrated in Fig. 1(e). A Higher corrosion temperature will naturally introduce faster oxide development, accompanied by accumulated growth stress, which may be released by crack initiation and propagation through the scale.

The cross-sectional morphology of the sample exposed to SCW at 550 ℃ and 25 MPa for 1000 h, and the corresponding composition profiles determined by EDS, are shown in Figs. 2 and 3. The oxide scale was mainly composed of two different layers,

along with an innermost internal oxidation zone, which is in the bulk alloy and close to the oxide/metal interface. The outer layer between points labeled 1 and 2 has an approximate thickness of 12 μm, which is enriched in Fe and depleted in Cr. The inner

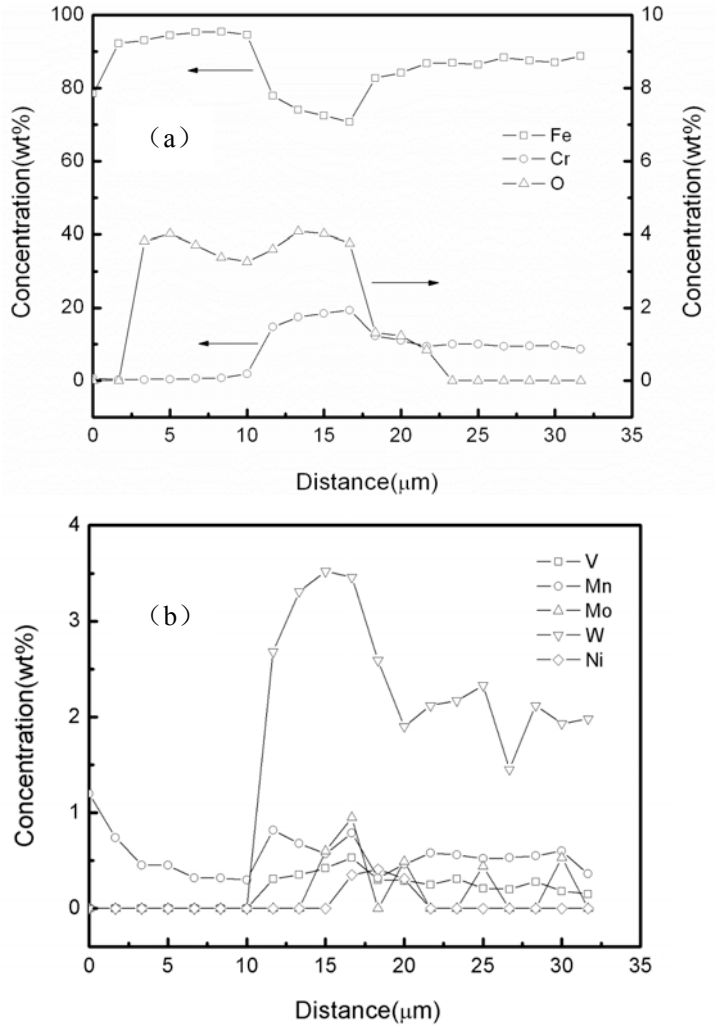

Fig. 3 Composition profiles of (a) major elements Fe, Cr, O, and (b) trace elements W, Mo, V, Ni, Mn across the oxide thickness of the sample exposed to SCW at 550 ℃ and 25 MPa for 1000 h.

layer between the points labeled 2 and 3 has an approximate thickness of 8 μm, where both Fe and Cr are enriched. The innermost internal oxidation zone between the points labeled 3 and 4 has an approximate thickness of 5 μm, which is charactered by a gradual variation of the concentration alloying elements and oxygen from the oxide

to the matrix. In addition to the major elements Fe, Cr and O, trace elements such as W, Mo, V, Ni and Mn were also detected due to their importance in alloy design, as described in the introduction. W, Mo and V were found to be enriched in the inner layer while they were depleted in the outer layer. Ni was enriched at the interface between the oxide and substrate, and depleted in

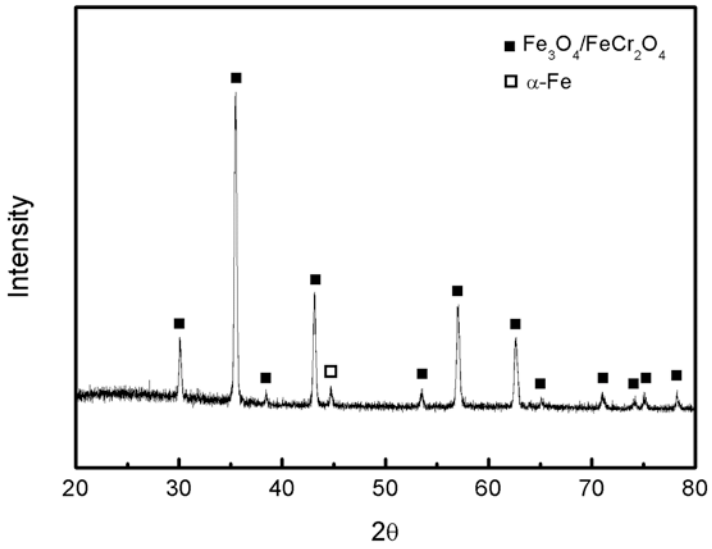

Fig. 4 XRD pattern of the sample exposed to SCW at 550 ℃ and 25 MPa for 1000 h.

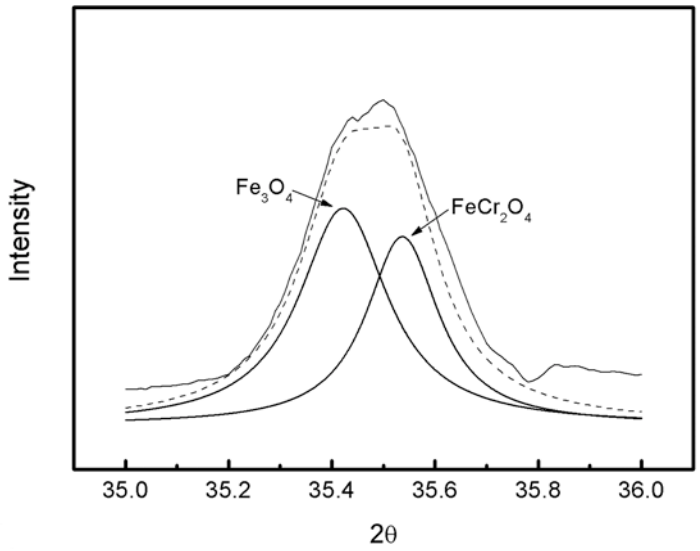

Fig. 5 Magnified overlapping local XRD peaks around 35.5° (2θ) in Fig. 4.

the oxide layer. Mn is enriched in the inner layer, but with a concentration in the outer oxide layer close to that in the matrix. Based on the current investigations, no conclusions can be drawn on the correlation between the Mn content and the corrosion behavior of F/M steels [27, 28].

The different distribution of alloying elements is attributed to their different affinities for oxygen and outward diffusion rates in the scale [29]. The oxidation probably proceeds as follows. Firstly, Cr and Fe are oxidized by reacting with diffused oxygen to form an inner Fe/Cr-mixed oxide layer. Simultaneously, the formation of this layer would lower the oxygen potential at the oxide/metal interface, making Fe oxide less stable, resulting in outward diffusion of Fe and formation an outer Fe oxide layer. The formation of the inner oxide layer, acting as a barrier against the diffusion of metals and oxygen, would hamper further development of the scale. W, Mo and V are enriched in the inner oxide layer due to their relatively immobility through the barrier layer.

The XRD pattern of the sample exposed at 550 □ and 25 MPa for 1000 h is shown in Fig. 4, in which the peaks for magnetite (Fe_3O_4) and/or spinel ($FeCr_2O_4$) are observed. The magnified peaks around 35.5° (2θ) shown in Fig. 5 indicate the existence of both magnetite and mixed Fe-Cr oxides with a spinel structure in the scale, which overlap to some extent. Combination of XRD and SEM/EDS analyses suggest that the outer Fe-rich layer is probably magnetite, while the inner Fe/Cr-rich layer is a mixture of magnetite and a Fe- Cr oxide with a spinel structure.

The weight gain versus exposure time is plotted in Fig. 6. The oxidation at 600 □

was more severe than that at 500 and 550 ℃. Since the test time (several weeks) is much shorter than the service time (tens of years) of nuclear reactors, an extrapolation based on fitting available experimental data is needed to provide a reasonable prediction oxide growth with prolonged exposure. The experimental weight gain data can be fitted using the following equation [7]:

$$WG = A' t^n \quad (1)$$

where WG is the weight change of P92 in mg/dm^2, A' is rate constant in mg/dm^2/h, t is exposure time in h, and n is an exponent describing the time dependence of the oxide growth. Both A' and n are shown in Fig.6. The weight gain data indicate a parabolic oxidation law.

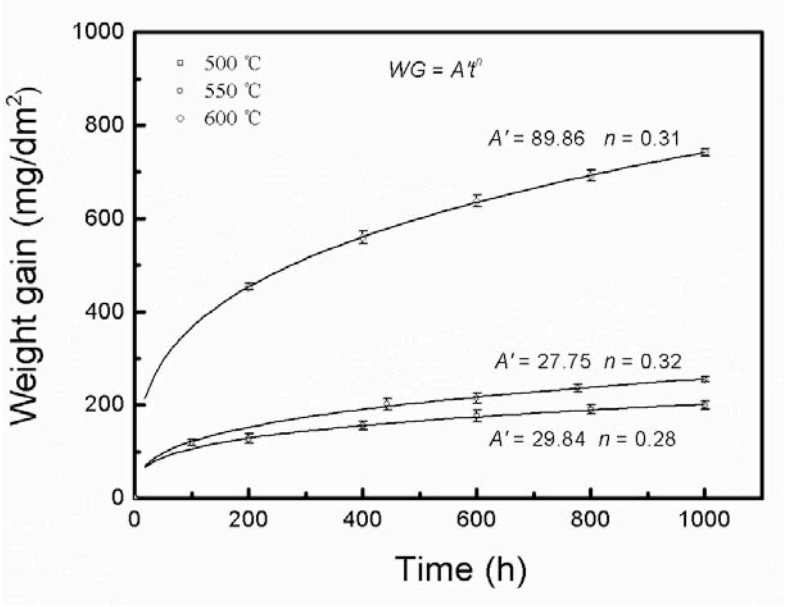

Fig. 6 Weight gain as a function of exposure time obtained from the samples exposed to SCW at 500 to 600 ℃ and 25 MPa.

The weight gain versus oxide thickness is plotted in Fig. 7, and follows a linear function. Since the weight gain is mainly induced by oxygen trapped in the oxide scale, the linear proportionality indicates that the scale density is nearly constant.

Weight gain occurred due to oxygen absorption during exposure, which was estimated by the following equation:

$$\Delta G_O = \rho_{outer} v_{outer} S(M_{O-outer} / M_{Fe_3O_4}) + \rho_{inner} v_{inner} S(M_{O-inner} / M_{Fe_3O_4-FeCr_2O_4}) \quad (2)$$

where ΔG_O is the amount of absorbed oxygen, ρ_{outer} and ρ_{inner} are the outer and inner layer densities respectively, v_{outer} and v_{inner} are the outer and inner layer thicknesses,

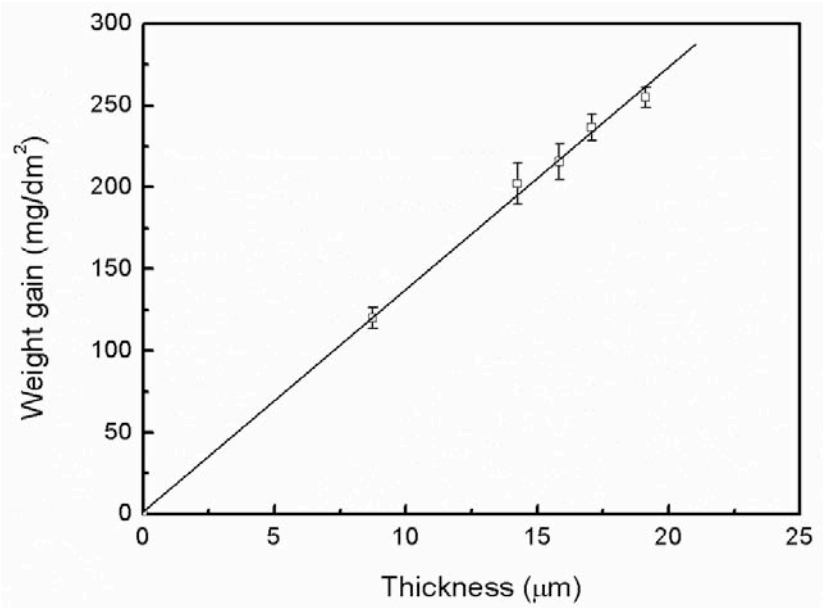

Fig. 7 Weight gain as a function of scale thickness for the samples exposed to SCW at 550 ℃ and 25 MPa.

respectively, $M_{O\text{-}outer}$ and $M_{O\text{-}inner}$ are the mole masses of oxygen in Fe_3O_4 and Fe_3O_4-$FeCr_2O_4$, respectively, $M_{Fe_3O_4}$ and $M_{Fe_3O_4-FeCr_2O_4}$ are the mole masses of Fe_3O_4 and Fe_3O_4-$FeCr_2O_4$, respectively, and S is the surface area of the exposed sample. Although the precise fraction of each oxide type in the Fe_3O_4-$FeCr_2O_4$ binary oxide was unknown, there is no significant difference between the densities of Fe_3O_4 and $FeCr_2O_4$. Therefore the ratio of Fe_3O_4 and $FeCr_2O_4$ was assumed to be 1:1, which would not result in any significant error concerning the current evaluation of the absorbed oxygen amount. Taking the sample exposed at 550 ℃ and 25 MPa for 1000 h

for example, calculations are based on equation 2, in which all the related parameters are available. $M_{O\text{-}outer}$, $M_{O\text{-}inner}$, $M_{Fe_3O_4}$ and $M_{Fe_3O_4-FeCr_2O_4}$ are already known. v_{outer} and v_{inner} are obtained from SEM observations. S is based on the dimensions of the samples. ρ_{outer} and ρ_{inner} are taken from previous work [30]. The results and related parameters in this calculation are listed in Table 2. The calculated amount of oxygen absorbed in the scale was 43.01 mg, very close to the measured weight gain (42.80 mg). This implies that the corrosion behavior of the P92 steel in SCW is similar to that in gaseous environment where only solid growth takes place without any metallic dissolution, which is in accord with the results by Yi [30].

Table 2 Estimation the amount of absorbed oxygen in the surface oxide

	Inner oxide layer	**outer oxide layer**
Oxide	*Fe_3O_4-$FeCr_2O_4$ binary (1:1)*	*Fe_3O_4*
Thickness (μm)	*9.18*	*9.94*
Surface area (mm^2)	*1602.00*	*1602.00*
Density (g/cm^3)	*4.91*	*5.17*
O content in oxide (wt. %)	*28.10*	*27.60*
O absorbed (mg)	*20.29*	*22.72*
Calculated total O absorbed (mg)	*43.01*	
Measured weight gain (mg)	*42.80*	

4. Conclusions

The corrosion response of ferritic/martensitic steel P92 was tested in SCW at 500

to 600 ℃ and 25 MPa with a dissolved oxygen content below 10 ppb for up to 1000 h. A dual-layered oxide scale, which composed of an outer magnetite layer and an inner magnetite/Fe-Cr spinel mixed oxide layer, formed on P92. The initial oxide scale had a rather high porosity, which decreased with the exposure time. Oxidation rates of all the samples followed a parabolic law, and the time exponent *n* increased with the exposure temperature. The corrosion at 600 ℃ was so severe that cracks occurred along the oxide grain boundaries in the scale. The corrosion mechanism for P92 exposed in SCW is proposed to be absorption of oxygen without metallic dissolution, similar to gas-phase oxidation.

Acknowledgement

The financial support by the National Basic Research Program of China (2007CB209800) is gratefully acknowledged.

References

[1] D. Squarer, T. Schulenberg, D. Struwe, Y. Oka, D. Bittermann, N. Aksan, C. Maraczy, High performance light water reactor, Nucl. Eng. Des. 221 (2003) 167-180.

[2] A Technology Roadmap for Generation IV Nuclear Energy Systems, Report No. GIF002-00, 1 December, 2002 (http://nuclear.gov/).

[3] K.H. Mayer, New materials for improving the efficiency of fossil-fired thermal power stations, in: International Joint Power Generation Conference, PWR-vol. 33, ASME, 1998, p. 831.

[4] M. Bethmont, Damage and lifetime of fossil power plant components, Mate. High Temp. 15 (1998) 231-237.

[5] M. Schütze, M. Schorr, D.P. Renusch, A. Donchev, J.P.T. Vossen, The role of alloy composition environment and stresses for the oxidation resistance of modern 9% Cr steels for fossil power stations, Mater. Res. 7 (2004) 111-120.

[6] T.R. Allen, Workshop on Higher Temperature Materials for Advanced Nuclear Energy

Systems, DOE Office of Nuclear Energy, Science and Technology, La Jolla, CA, March 18, 2002.

[7] X. Ren, K. Sridharan, T.R. Allen, Corrosion of ferritic-martensitic steel HT9 in supercritical water, J. Nucl. Mater. 358 (2006) 227-234.

[8] M.C. Sun, X.Q. Wu, Z.E. Zhang, E.H. Han, Analyses of oxide films grown on Alloy 625 in oxidizing supercritical water, J. Supercri. Fluids 47 (2008) 309-317.

[9] X. Gao, X.Q. Wu, Z.E. Zhang, H. Guan, E.H. Han, Characterization of oxide films grown on 316L stainless steel exposed to H_2O_2-containing supercritical water, J. Supercri. Fluids 42 (2007) 157-163.

[10] L. Tan, X. Ren, K. Sridharan, T.R. Allen, Corrosion behavior of Ni-base alloys for advanced high temperature water-cooled nuclear plants, Corros. Sci. 50 (2008) 3056-3062.

[11] S.H. Son, J.H. Lee, C.H. Lee, Corrosion phenomena of alloys by subcritical and supercritical water oxidation of 2-chlorophenol, J. Supercri. Fluids 44 (2008) 370-378.

[12] L. Tan, X. Ren, K. Sridharan, T.R. Allen, Effect of shot-peening on the oxidation of alloy 800H exposed to supercritical water and cyclic oxidation, Corros. Sci. 50 (2008) 2040-2046.

[13] Y. Chen, K. Sridharan, T.R. Allen, Corrosion behavior of ferritic-martensitic steel T91 in supercritical water, Corros. Sci. 48 (2006) 2843-2854.

[14] P. Ampornrat, G.S. Was, Oxidation of ferritic–martensitic alloys T91, HCM12A and HT-9 in supercritical water, J. Nucl. Mater. 371 (2007) 1-17.

[15] G. Gupta, P. Ampornrat, X. Ren, K. Sridharan, T.R. Allen, G.S. Was, Role of grain boundary engineering in the SCC behavior of ferritic–martensitic alloy HT-9, J. Nucl. Mater. 361 (2007) 160-173.

[16] S.S. Hwang, B.H. Lee, J.G. Kim, J.S. Jang, SCC and corrosion evaluations of the F/M steels for a supercritical water reactor, J. Nucl. Mater. 372 (2008) 177-181.

[17] I. Betova, M. Bojinov, P. Kinnunen, S. Penttila, T. Saario, Surface film electrochemistry of austenitic stainless steel and its main constituents in supercritical water, J. Supercri. Fluids 43 (2007) 333-340.

[18] R.L. Klueh, D.R. Harries, High-chromium ferritic and martensitic steels for nuclear application, ASTM, West Conshohocken, PA, 2001.

[19] J.C. Vaillant, B. Vandenberghe, B. Hahn, H. Heuser, C. Jochum, T/P23, 24, 911 and 92: New

grades for advanced coal-fired power plants-Properties and experience, Int. J. Pressure Vessels Piping 85 (2008) 38-46.

[20] B. Kim, C. Jeong, B. Lim, Creep behavior and microstructural damage of martensitic P92 steel weldment, Mater. Sci. Eng. A 483-484 (2008) 544-546.

[21] J.S. Jang, Y.B. Lee, C.H. Han, Y.S. Yi and S.S. Hwang, Effect of Cr content on supercritical water corrosion of high Cr alloys, Mater. Sci. Forum 475-479 (2005) 1483-1486.

[22] M. Bojinov, L. Heikinheimo, T. Siirio and S. Tuurna, Characterization of corrosion films on steels after long-term exposure to simulated supercritical water conditions, in: Proceedings of ICAPP'05, 2005, p. 1799-1807.

[23] L. Tan, Y. Yang, T.R. Allen, Porosity prediction in supercritical water exposed ferritic/martensitic steel HCM12A, Corros. Sci. 48 (2006) 4234-4242.

[24] L. Tan, Y. Yang, T.R. Allen, Oxidation behavior of iron-based alloy HCM12A exposed in supercritical water, Corros. Sci. 48 (2006) 3123-3138.

[25] S.A. Bradford, in: Metals Handbook, Ninth Ed. Corrosion, vol. 13, ASM International, Metals Park, OH, 1987, p. 68.

[26] G.S. Was, P. Ampornrat, G. Gupta. Corrosion and stress corrosion cracking in supercritical water, J. Nucl. Mater. 371 (2007) 176-201.

[27] V. Lepingle, G. Louis, D. Allue, B. Lefebvre and B. Vandenberghe, Steam oxidation resistance of new 12%Cr steels: comparison with some other ferritic steels, Corros. Sci. 50 (2008) 10114-1019.

[28] I. Iordanova, K.S. Forcey, R. Harizanova, Y. Georgiev and M. Surtchev, Investigation of structure and composition of surface oxides in a high chromium martensitic steel, J. Nucl. Mater. 257 (1998) 126-133.

[29] G.E. Totten, M.A.H. Hows, Steel Heat Treatment Handbook, Marcel Dekker, New York, 1997.

[30] Y.S. Yi, B.H. Lee, S.H. Kim, J.S. Jang, Corrosion and corrosion fatigue behaviors of 9Cr steel in a supercritical water condition, Mater. Sci. Eng. A 429 (2006) 161-168.